Transportation Research Part C 128 (2021) 103121

Contents lists available at ScienceDirect

Transportation Research Part C

journal homepage: www.elsevier.com/locate/trc

A linear Lagrangian model predictive controller of macro- and micro- variable speed limits to eliminate freeway jam waves☆

Yu Han [a,b], Meng Wang [c], Ziang He [a,b], Zhibin Li [a,b], Hao Wang [a,b], Pan Liu [a,b,*]

[a] School of Transportation, Southeast University, Nanjing, China
[b] Jiangsu Key Laboratory of Urban ITS, Jiangsu Province, China
[c] Department of Transport and Planning, Delft University of Technology, the Netherlands

ARTICLE INFO

Keywords:
Variable speed limits
Jam wave
Lagrangian model
Model predictive control
Connected automated vehicles

ABSTRACT

Variable speed limits (VSLs) are a common traffic control measure to resolve freeway jam waves. State-of-the-art model predictive control (MPC) approaches of VSLs are developed based on Eulerian Lighthill-Whitham and Richards (LWR) models, where the decision variables are flows between road segments. It is difficult to implement constraints on speeds that are necessary in typical real-world speed limit systems, because converting flow to speed results in nonlinear and non-convex optimization formulations. In this paper, we develop a new MPC of VSLs based on a discrete Lagrangian LWR model, in which the decision variables are average speeds of vehicle groups. This allows formulating speed constraints as control constraints rather than state constraints in the MPC problem. The optimization of vehicle groups speeds is formulated as a linear programming problem which can be solved efficiently. We further integrate the presented MPC to a hierarchical VSL control framework leveraging connected vehicles. The presented MPC decides the optimal target speed of each vehicle group led by a connected automated vehicle (CAV) at the upper macroscopic level with a prediction horizon of 20 min. At the lower microscopic level, CAVs randomly distributed in mixed traffic are regarded as actuators of the upper layer. Microscopic CAV accelerations are optimized in a short horizon of the order 5–10 s so that the human-driven vehicles following them reach the target speed from the upper layer in an efficient and smooth manner. The presented MPC and the hierarchical control approach are tested in microscopic simulation environments. Simulation results show that (i) the presented MPC resolves freeway jam waves efficiently with reasonable safety constraints implemented, and (ii) the presented hierarchical control approach can effectively resolve jam waves in a single-lane freeway, even though the penetration rate of CAVs is as low as 5%.

1. Introduction

Traffic control has gained substantial attention as an cost-effective means to deal with congestion on freeways (Papageorgiou et al., 2003). Variable speed limits (VSLs) have emerged as a popular control measure for freeway traffic operation. VSLs are often applied at the upstream of a freeway bottleneck to regulate the mainstream arriving flow to the bottleneck, such that traffic breakdown can be prevented/delayed or traffic jams can be eliminated. Compared to ramp metering, it has the potential to refrain the control actions on

☆ This article belongs to the Virtual Special Issue on IG005584: VSI:ISTTT24.

* Corresponding author.
E-mail addresses: yuhan@seu.edu.cn (Y. Han), liupan@seu.edu.cn (P. Liu).

https://doi.org/10.1016/j.trc.2021.103121
Received 24 December 2020; Received in revised form 9 March 2021; Accepted 3 April 2021
Available online 12 May 2021

freeways without influencing the underlying urban network.

In the literature, a large number of studies have demonstrated that VSLs are effective to improve freeway traffic operation efficiency (Papageorgiou et al., 2003; Hegyi et al., 2005; Jin and Jin, 2015). In general, there are two mechanisms of VSLs in regulating mainstream flows. First, VSLs below the critical speed lead to a fundamental diagram that has lower capacity than normal conditions. Therefore, the application of VSLs upstream of a bottleneck permanently reduces the mainstream arriving flow, which avoids the bottleneck activation. The second mechanism is applicable when a jam is already formed. When lower VSLs are applied on a freeway stretch at under-critical densities, there is a transition to a new traffic state, which serves the same flow at lower speed and higher density. During this transition, the density increase leads to a temporary reduction of the mainstream flow. Traffic jams are gradually resolved if the inflows to the jams are lower than the outflows.

The VSL control strategies developed based on the first mechanism are often used for deactivating infrastructural bottlenecks, e.g., on-ramp, lane-drop, workzones, sags. There are various theories and algorithms to determine the appropriate values of the VSLs. Studies of Chen et al. (2014), Chen and Ahn (2015) developed analytical approaches of VSLs based on the kinematic wave theory for recurrent and non-recurrent infrastructural bottlenecks. It was assumed that VSL-induced traffic states are stable on the congestion branch of the fundamental diagram. Carlson et al. (2011) developed a feedback based VSL control strategy to keep the density of the target bottleneck at the critical value by regulating the mainstream flow. Similar control designs for other infrastructural bottlenecks were presented in (Jin and Jin, 2015; Papamichail et al., 2018). Model predictive control (MPC) approaches, which predict the evolution of traffic dynamics and decide the optimal control scheme for the time period in which the relevant traffic dynamics occur, are very popular for VSLs strategies. Hegyi et al. (2005) and Carlson et al. (2010) presented MPC approaches of VSLs that are based on a non-linear second-order traffic flow model METANET (Messmer and Papageorgiou, 1990; Kotsialos et al., 2002). Studies of Muralidharan and Horowitz (2015), Roncoli et al. (2015), Hadiuzzaman and Qiu (2013) developed simpler MPC approaches that have less computational complexity based on the cell transmission model and its variants. For MPC approaches, the accuracy of prediction models may play an important role in improving traffic performance. Han et al. (2020) found that the mismatch between the prediction model and the process model may result in inferior traffic performance. The study of Li et al. (2017) presented a reinforcement learning based approach of VSLs to maximize the throughput of on-ramps bottlenecks. The VSL agent is trained to learn the optimal control actions through an offline traffic simulation.

The VSL control strategies developed based on the second mechanism usually apply to resolve jam waves after their formation. A jam wave, also known as wide moving jam or shock wave in some studies, e.g., (Lighthill and Whitham, 1955; Kerner and Rehborn, 1996; Hegyi et al., 2005; Treiber and Kesting, 2013), usually originates from traffic breakdown in a high-demand traffic flow situation, and propagates upstream with both the jam head and the jam tail. There are also different theories and algorithms to determine the appropriate values of the VSLs to resolve jam waves. Hegyi et al. (2008) presented an analytical approach of VSLs, The SPECIALIST algorithm, that was developed based on the LWR theory (Lighthill and Whitham, 1955) to resolve freeway jam waves. It was successfully tested in practice and the testing results were evaluated in some studies (Hegyi and Hoogendoorn, 2010; Han et al., 2015). As the SPECIALIST algorithm has a feed-forward structure, disturbances during the activation of the VSLs cannot be handled. The algorithm was later extended to a feedback structure, which is known as COSCAL v2, to better handle disturbances (Mahajan et al., 2015). Wang et al. (2012) presented a simulation-based approach to find appropriate lower bounds of VSLs that can avoid the formation of new jam waves induced by VSLs. Hegyi et al. (2005) presented a model predictive control (MPC) approach of VSLs, where the design was based on the METANET model with VSLs extension. Due to the non-convex optimization formulation of METANET-based MPC, the solution may depend on the selection of the initial guess trajectory. In other words, the solution of the optimization may get stuck at a local minimum if the initial guess is not appropriately chosen. Han et al. (2017b) designed a MPC of VSLs based on an extended discrete LWR model that can accurately reproduce the capacity drop. The computational efficiency was significantly improved compared to the METANET-based MPC, as a result of the linear quadratic formulation of the optimization. However, it is difficult to implement safety constraints to the MPC, which are necessary in typical real-world speed limit systems.

Although VSLs strategies for improving traffic operation efficiency have been widely investigated in the literature, to date only a few of them have been implemented to practice. The fact that most of the VSLs strategies have not been implemented to the field may be attributed to the following knowledge gaps. First, some VSLs strategies are developed based on strong assumptions that are difficult to be validated. For example, the assumption that sub-critical VSLs lead to lower capacity with lower VSLs, which was used in many VSL strategies for deactivating infrastructural bottlenecks, may not work in all cases. Papageorgiou et al. (2008) found that the VSL-induced capacity may be lower than the free-flow capacity. At a different site, Soriguera et al. (2017) could not identify any permanent flow reduction that could be attributed to VSLs, even when the speed limit value is as low as 40 km/h. Second, the MPC of VSLs with nonlinear and non-convex optimization formulations may suffer from too high computational costs, which make them difficult to be implemented for online traffic control. Last but not least, many studies have demonstrated their VSL control strategies using same models as the prediction model and the process model which represents the reality. In field applications, there is inherently significant mismatch between the dynamics of the prediction model and the process. Therefore, those control strategies also need to be tested using different models to represent the reality, so as to increase the confidence that they will also robustly work in practice under model mismatch.

In recent years, with the development of connected and automated vehicle (CAV) technology, some studies designed microscopic speed limit control approaches to improve traffic operations using CAVs as actuators. One stream of study focused on speed harmonization concept that aims to reduce temporal and spatial variations of traffic speed with certain traffic control approaches such as variable speed limits (VSL) and/or CAVs (Khondaker and Kattan, 2015; Ma et al., 2016; Ghiasi et al., 2019; Talebpour et al., 2013). Since CAVs have the potential to stabilize traffic flow and dissipate stop-and-go waves (Liu et al., 2018; Wang et al., 2015; Tian et al., 2019), they become a natural option for speed harmonization studies. However, it has been generally agreed that the benefit of vehicle-

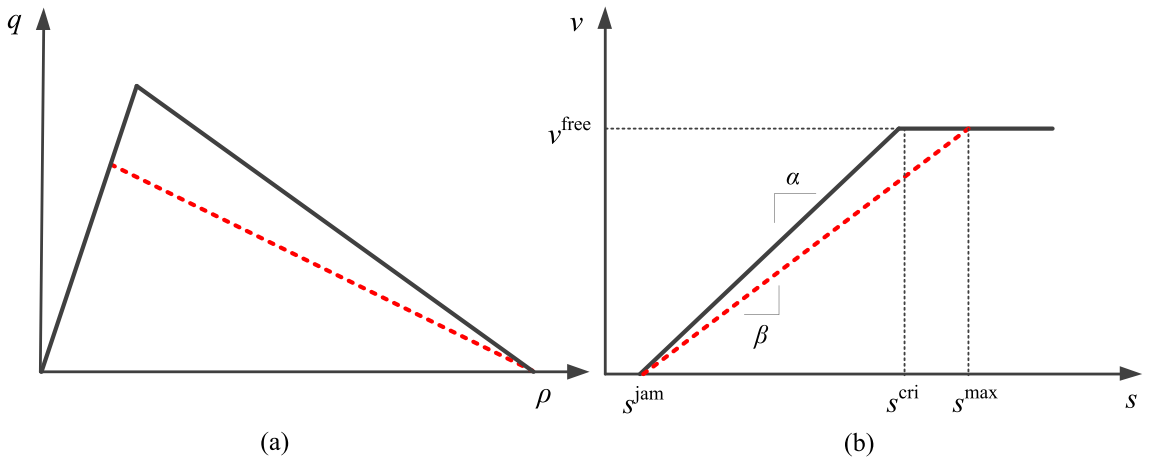

Fig. 1. The fundamental diagram in Eulerian coordinates (left) and in Lagrangian coordinates (right).

to-vehicle (V2V) based CAVs in enhancing capacity and flow stability is marginal in low market penetration rates (Liu et al., 2018) and traffic control layer is necessary in these conditions (Roncoli et al., 2015; Wang et al., 2016). Consequently, it is still a challenge to design integrated traffic and CAV control systems at very low market penetration rates.

This paper presents a model predictive control approach of VSLs that fills the aforementioned gaps and offers a proof-of-concept for integrated traffic and vehicle control in mixed CAV and human-driven vehicle environment. The proposed VSL control approach is built upon the second mechanism of VSLs in regulating mainstream flows, which has been validated in (Han et al., 2017a). The optimization in the proposed MPC is formulated as a linear programming problem, which can be solved efficiently. Moreover, the presented approach is tested in microscopic simulation to demonstrate robustness to modeling mismatch.

The contribution of this paper is twofold. First, a new MPC controller of VSLs is developed based on an extended discrete Lagrangian LWR model. The extended model keeps the linear property of the original discrete Lagrangian LWR model, meanwhile taking capacity drop and VSLs effects into account. Unlike conventional discrete LWR model-based MPC of VSLs (e.g., Han et al. (2017b)) based on Eulerian models, where the decision variables are flows between road segments, the proposed MPC is able to implement safety constraints straightforward to the optimization, as the decision variables are average speeds of vehicle groups. Secondly, a hierarchical VSL control approach that can be applied to a CAV environment is designed. The presented MPC decides the optimal speed of each vehicle group at the upper level in a horizon of around 20 min. At the lower level, speed trajectories of a small amount of randomly distributed CAVs are optimized in a short horizon of the order 5–10 s so that the human-driven vehicles following them reach the target speed efficiently and smoothly.

The rest of this paper is organized as follows. Section 2 presents the extended discrete Lagrangian LWR model. A numerical experiment is conducted to show that the presented model is able to reproduce VSL-related traffic phenomena that are critical for resolving freeway jam waves. The MPC controller developed based on the presented model is presented in Section 3, where the optimization formulation is specified. In Section 4, we present the hierarchical VSL control design, and specifically elaborate the lower level controller which optimizes the speed trajectories of CAVs. Section 5 describes the design of the simulation experiments, in which the presented MPC control approach and the hierarchical VSL control approach are investigated. A discussion and some topics for future research conclude the paper in Section 6.

2. The discrete Lagrangian LWR model

We present the Lagrangian LWR model and propose extension for capacity drop and VSLs in this section.

2.1. Original discrete LWR models

The LWR model, which was developed based on the hydrodynamic theory, can be discretized in Eulerian coordinates (time t, space x) and Lagrangian coordinates (time t, vehicle number n) for numerical traffic simulation and traffic prediction purposes. In Eulerian coordinates, the traffic network is divided into cells, and traffic states are represented by the densities of the cells at discrete time steps. The density of cell i at time step t, which is represented as $\rho_i(t)$, is updated as:

$$\rho_i\left(t+1\right) = \rho_i\left(t\right) + \frac{\Delta t}{l_i}\left(q_{i-1}(t) - q_i(t)\right), \tag{1}$$

where Δt is the duration of discrete time steps, and l_i is the length of cell i. q_{i-1} and q_i denote the inflow and outflow of cell i respectively. q_i is determined as the minimum value between the sending flow of cell i and the receiving flow of its downstream cell, whose upper bounds are specified by the fundamental diagram representing the equilibrium flow-density relation. The original

discrete first-order traffic flow model, i.e, the CTM (Daganzo, 1994), assumes a triangular fundamental diagram which is depicted as the solid lines in Fig. 1 (a).

The original CTM was extended to account for capacity drop Han et al. (2016). It was assumed that the traffic states of discharging flows from congestion are represented by the red dashed line with a fixed slop in Fig. 1 (a). This implies increasing severity of congestion results in decreasing discharge rates, evidenced by the empirical study of Yuan et al. (2015). Owing to the linear property, the model has been developed to a linear quadratic MPC of VSLs that can be efficiently solved (Han et al., 2017b).

In Lagrangian coordinates, the vehicles on a freeway are divided into vehicle groups, which are increasingly numbered from downstream to upstream. The original discrete Lagrangian LWR model, presented by Leclercq et al. (2007), defined traffic states as the average spacing of vehicle groups. The average spacing of vehicle group j, $s_j(t)$, is represented as,

$$s_j\left(t\right) = \frac{x_{j-1}\left(t\right) - x_j\left(t\right)}{\Delta n} \tag{2}$$

where $x_j(t)$ denotes the spatial location of the most upstream vehicle in group j, i.e. platoon tail. Δn is the number of vehicles in a group. The average spacing, $s_j(t)$, is updated as:

$$s_j\left(t+1\right) = s_j\left(t\right) + \left(v_{j-1}\left(t\right) - v_j\left(t\right)\right) \cdot \frac{\Delta t}{\Delta n}. \tag{3}$$

where $v_j(t)$ is the average speed of vehicle group j. The upper bounds of $v_j(t)$ are specified by the Lagrangian fundamental diagram, which represents the equilibrium relation between the spacing and the speed. The Lagrangian fundamental diagram is characterized by three parameters, which are the free-flow speed v_j^{free}[m/s], the critical spacing s_j^{cri}[m], and the jam spacing s_j^{jam}[m]. The solid lines in Fig. 1 (b) show the Lagrangian fundamental diagram, which is consistent with the triangular fundamental diagram in Fig. 1 (a). The slope of the left line is denoted as α, and

$$\alpha = \frac{v_j^{\text{free}}}{s_j^{\text{cri}} - s_j^{\text{jam}}}. \tag{4}$$

If $s_j(t)$ is given, the average speed, $v_j(t)$, is calculated according to:

$$v_j\left(t\right) = \min\left(v_j^{\text{free}}, \alpha \cdot \left(s_j\left(t\right) - s_j^{\text{jam}}\right)\right). \tag{5}$$

Discrete traffic flow models should always satisfy the Courant-Friedrichs-Lewy (CFL) condition (Courant and Friedrichs, 1999) to guarantee stable numerical solutions. In Lagrangian coordinates, the CFL condition reads:

$$\frac{\Delta t}{\Delta n} \cdot \alpha \leqslant 1. \tag{6}$$

Physically, it means that the distance a vehicle group can travel downstream within one time step need to be restricted. Although the fundamental diagrams shown in Fig. 1 have the same physical interpretation, it has been demonstrated that there is less numerical diffusion when solving the LWR model in Lagrangian coordinates compared with using Eulerian coordinates (Leclercq et al., 2007; Yuan et al., 2012).

2.2. Model extension with capacity drop and VSLs

The original discrete Lagrangian LWR model does not account for capacity drop. To reproduce the capacity drop, we extend the model by assuming that the spacing of a vehicle group in discharging flows from congestion is linearly related the speed in congestion (Han et al., 2016). A new parameter, the maximum spacing, $s_j^{\max}$, is introduced to represent the spacing of vehicle groups moving out from a traffic jam that is in full stop. The slope of the red dashed line in Fig. 1 (b), which is denoted as β, has a fixed value:

$$\beta = \frac{v_j^{\text{free}}}{s_j^{\max} - s_j^{\text{jam}}}. \tag{7}$$

For a vehicle group j moving out from a traffic jam, depending on the speed in the jam, the spacing of that vehicle group at the time when its speed recovers to the free-flow speed is larger than the critical spacing (but no larger than the maximum spacing) and is dependent on the speed in the jam. Therefore, at the downstream of a traffic jam, the traffic flow is in a such a state that the speed is equal to the free-flow speed and the density is lower than the critical density, which reproduces the capacity drop. The dashed line in Fig. 1 (b) is dominating in determining the speed of a vehicle group if the vehicle group is accelerating,

$$v_j\left(t\right) = v_j\left(t-1\right) + \beta \cdot \left(s_j\left(t\right) - s_j^{\text{eq}}\left(t-1\right)\right), \text{ if } v_j\left(t\right) > v_j\left(t-1\right) \tag{8}$$

where $s_j^{\text{eq}}(t-1)$ denotes the equilibrium spacing of the speed $v_j(t-1)$:

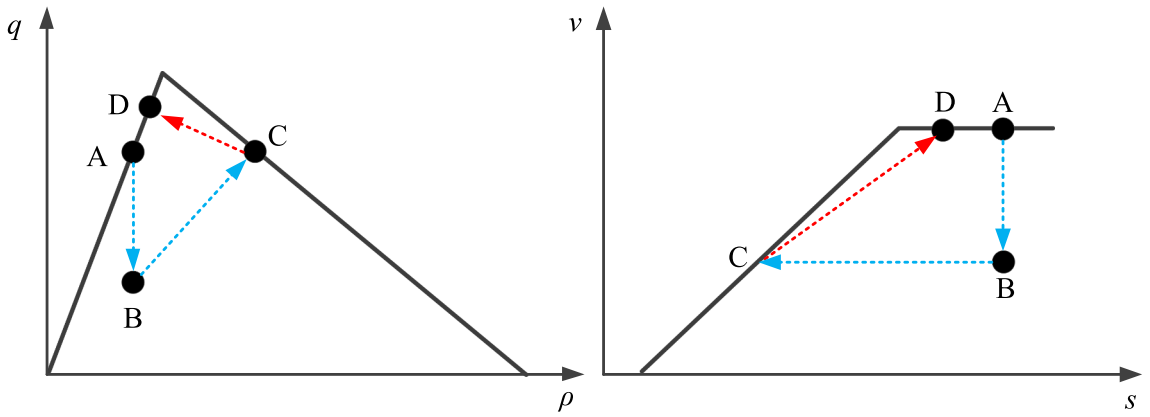

Fig. 2. Traffic state transitions under speed limit control in two fundamental diagrams. Blue dashed lines represent traffic state transitions from a free flow state to an equilibrium VSL-controlled state. Red dashed lines represent the state change after releasing the VSL control. (For interpretation of the references to colour in this figure legend, the reader is referred to the web version of this article.)

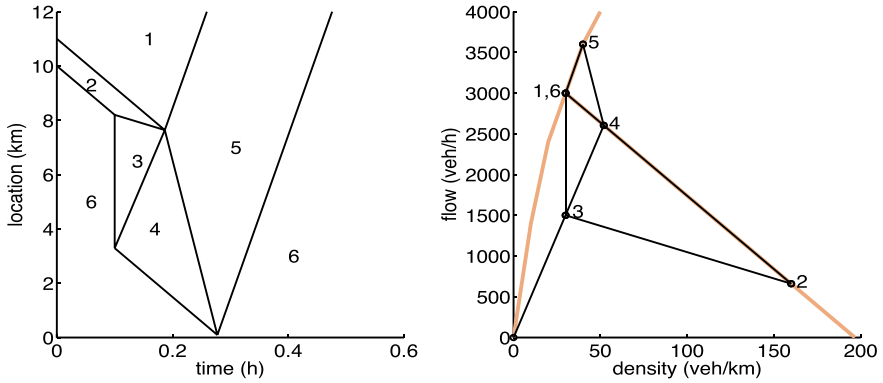

Fig. 3. Illustration of traffic evolution under the SPECIALIST (Hegyi et al., 2008). The left figure is the time–space graph and the right figure is the fundamental diagram.

$$s_j^{\mathrm{eq}}\left(t-1\right)=\frac{v_j\left(t-1\right)}{\alpha}+s_j^{\mathrm{jam}}. \tag{9}$$

The model is also extended to reproduce the traffic dynamics under VSLs. If the values of VSLs displayed to a group of vehicles are known, the average speed of the vehicle group is calculated as,

$$v_j\left(t\right)=\min\left(v_j^{\mathrm{free}},\alpha\cdot\left(s_j\left(t\right)-s_j^{\mathrm{jam}}\right),\left(1-\frac{\beta}{\alpha}\right)\cdot v_j\left(t-1\right)+\beta\cdot\left(s_j(t)-s_j^{\mathrm{jam}}\right),\left(1+\theta\right)\cdot v_j^{\mathrm{control}}\left(t\right)\right), \tag{10}$$

where $v_j^{\mathrm{control}}(t)$ is the speed limit value displayed to vehicle group j at time t. $1+\theta$ is the non-compliance factor that expresses that drivers usually do not fully comply with the displayed speed limit and their target speed are usually higher than what is displayed. In Eq. (10), the first two terms correspond to Eq. (5), which decides the speed of a vehicle group if it is in an equilibrium state, and the third term corresponds to Eq. (8), which calculates the speed when the vehicle group is accelerating.

2.3. The mechanism of VSLs against jam waves

Although there are different theories and methods to determine the optimal values of VSLs for jam waves' suppression, their mechanisms are similar. When a lower VSL is applied on a freeway stretch with an under-critical traffic density, the traffic shifts to a new state, which serves the same flow at lower speed and higher density. During this transition, the density increase leads to a temporary reduction of the mainstream flow. Jam waves are gradually resolved if the inflows to the jams are lower than the outflows.

Fig. 2 depicts the transitions of VSL-induced traffic state on two fundamental diagrams in both Eulerian coordinates and Lagrangian coordinates. In the Eulerian fundamental diagram, the dots and the dashed lines represent traffic state transitions of a roadway segment under speed limit control. Before activating the speed limit, the segment is in a free-flow state represented by A. The state changes to B, which has the same density as A but a lower speed, as soon as the speed limit is activated. As time advances, the state

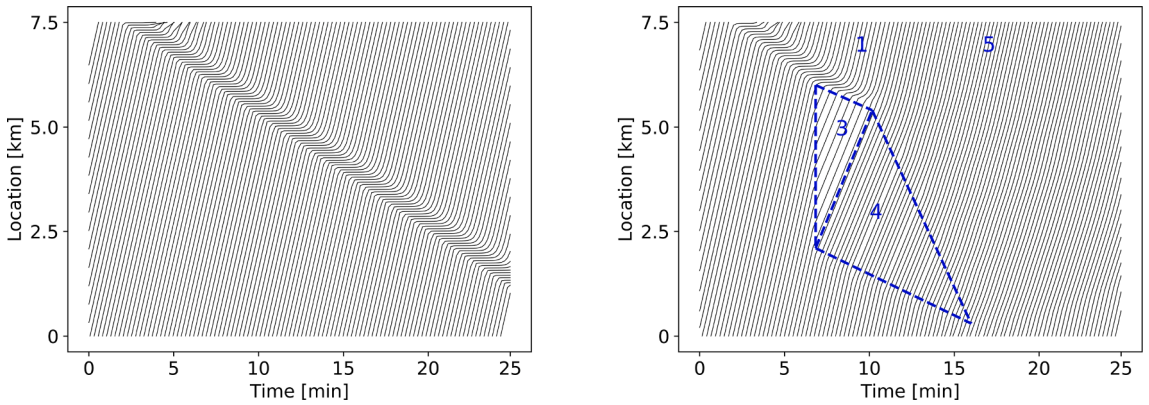

Fig. 4. The left figure is the trajectories of all the vehicle groups without VSL control, and right figure is the trajectories of all the vehicle groups under the SPECIALIST control. Inside the blue dashed areas is the VSL control area generated by SPECIALIST.

changes to C, which has the same flow as A and the speed as B. Once the speed limit control is deactivated, traffic state goes to D, which has a free-flow speed and a discharging flow close to the free-flow capacity.

The dots and the dashed lines in the Lagrangian fundamental diagram represent traffic state transitions of a vehicle group travelling through a speed limit-controlled area. Before entering the VSL area, traffic state of the vehicle group is in a free-flow state represented by A. As soon as it reaches to the speed limit control area, the vehicle group turns to state B, which has the same value of spacing as A and lower value of speed. In the control area, the vehicle group travels at a constant speed while its spacing between group members decreases gradually. The state of the vehicle group changes to state C, which represents the homogeneous traffic state under the speed limit control. After the vehicle group moving out of the VSL area, its state goes to D, which has a free-flow speed and a discharging flow close to the free-flow capacity. Note the extension of the capacity drop applies here as well: i.e. how close D can restore to the capacity depends on the VSL value imposed in the control area and state B.

2.4. A numerical experiment

In this subsection, a simulation study is conducted to show how the model reproduces VSL-related phenomena. We use the extended Lagrangian LWR model to reproduce the SPECIALIST algorithm (Hegyi et al., 2008), which has been successfully tested in the field to resolve jam waves. Fig. 3 is used to explain the theory of SPECIALIST. The time–space graph in the left figure shows the traffic states on a road stretch and their propagation over time. The density-flow diagram in the right figure shows the corresponding density and flow values for these states. According to the shock wave theory, the boundary (front) between two states in the left figure has the slope as the slope of the line that connects the two states in the right figure. Area 2 represents a short jam wave that propagates upstream and which is surrounded by traffic in free-flow (area 1 and 6). As soon as the jam wave is detected, the speed limits upstream of the jam wave are switched on, where traffic state changes to state 3. The inflow of area 2, which is the flow of state 3, is lower than the outflow of area 2, which is the flow of state 1. Hence the size of the jam wave is decreasing as time advances. The required length of the speed-limited stretch to resolve the jam depends on the density and flow associated with state 2 and the physical length of the detected jam. When the jam wave is resolved there remains an area with the speed limits active (state 4) with a moderate density (higher than in free-flow, lower than in the jam wave). It is assumed that traffic leaving area 4 has a higher flow and a higher speed than state 4, which is represented by state 5. A basic assumption in the SPECIALIST theory is that the traffic from area 4 can flow out more efficiently than a queue discharging from full congestion as in the shock wave (flow of sate 2), which results in the increasing of the total throughput. In a later research, the analysis of the data from the SPECIALIST field test confirms this assumption (Hegyi and Hoogendoorn, 2010). For a full presentation of the concept, readers are referred to Hegyi et al. (2008).

A synthetic homogeneous freeway stretch, which is 7.5 km in length and contains three lanes, is used as the test bed for the numerical simulation. The presented model is utilized as the simulation model to reproduce the propagation of a jam wave, which is shown in the left figure in Fig. 4. Parameters of the model, which apply to all the vehicle groups, are set as follows: the free flow speed is set to 30 m/s, $s^{\text{jam}} = 8$ m, $s^{\text{cri}} = 50$ m, and $s^{\max} = 60$ m. Δt is set to 10 s, and Δn is set to 19 veh/group, which satisfies the CFL condition. These parameters give us a free-flow capacity of 2160 veh/h/lane, and the maximum capacity drop of 16.7%. The simulation lasts for 25 min. The demand is set to 5500 veh/h constantly for the entire simulation period. To reproduce a jam wave, we block the downstream boundary of the stretch for a short period of time (from min. 2 to min. 4).

The SPECIALIST algorithm is implemented in the simulation, and the VSL control areas are shown as the blue dashed areas in the right figure in Fig. 4. The value of speed limit is set to 60 km/h and all drivers are assumed to fully comply with the speed limit control. Simulation result shows that the proposed model can reproduce how the SPECIALIST algorithm, which has a similar VSL mechanism in resolving jam waves as the presenting approach, works under a deterministic traffic environment.

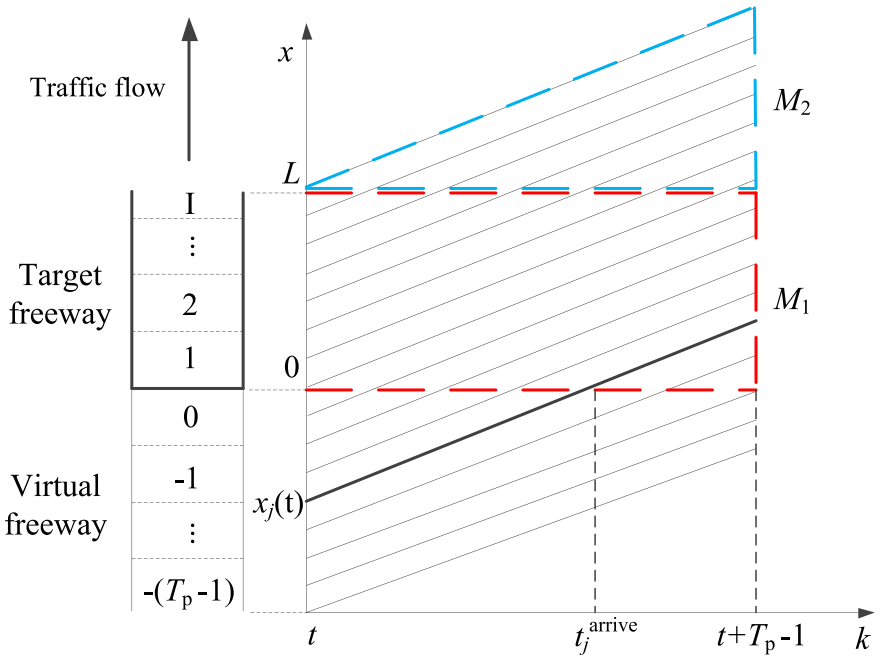

Fig. 5. The left part is a graphical interpretation of the target freeway and the "virtual freeway" in the presented VSL control problem. The right part shows some symbolistic trajectories, which explain the implication of M_1, and M_2 in the objective function.

3. Optimal VSL control with road-based sensors and actuators

The model presented in the previous section is developed to an optimal VSL formulation in an MPC framework. This sections presents the operation conditions, control formulation and a numerical example showing the workings of the MPC.

3.1. Operations of the MPC based VSL

MPC-based controllers predict traffic flow evolution by traffic flow models, and determine the optimal control signals based on current system state. The length of prediction horizon is represented by T_p, and the length of control horizon is represented as T_c. In linear MPCs, (e.g., Le et al. (2013), Roncoli et al. (2015), Han et al. (2017b)), T_c and T_p are usually in a same value. In the presented MPC, we also assume T_c is equal to T_p. The duration of a control time step is represented as T_k. After optimization the first sample of the optimal control signals is applied to the process. The control signal is recalculated again at the next time step in the receding horizon scheme (Mayne et al., 2000; Hegyi et al., 2005).

The input of a MPC controller for traffic systems include the estimated traffic state of a network, the predicted traffic demand, the boundary condition and disturbances. In the proposed MPC design, we do not consider disturbances explicitly. Nevertheless, we will test the proposed MPC under model mismatch. The workings of the proposed MPC requires that the downstream boundary is in free-flow condition. The traffic network we consider is a homogeneous freeway stretch, which is suitable for applying VSLs for jam wave suppression.

3.2. Traffic state dynamics

As presented in the previous section, traffic state of the Lagrangian model is represented by the average spacing of all vehicle groups. For freeways equipped with fixed sensors such as loop detectors, we first estimate the traffic state at fixed locations, i.e., in Eulerian coordinates, then reformulate the Eulerian traffic state to Lagrangian traffic state by the following method.

It is assumed that several fixed sensors measuring traffic counts and speeds divide a freeway stretch into cells, which are increasingly numbered from 1 to I from upstream to downstream, as shown in Fig. 5. The traffic demand of a future step $t+k$ predicted at time t is denoted as $d(t+k)$, which represents the traffic volume arriving to the freeway stretch at the kth time step in the prediction. To reformulate the traffic volume to Lagrangian traffic state, the predicted demand is distributed on a "virtual-freeway" at the upstream of the target freeway stretch. The "virtual-freeway" is divided into cells and the length of each cell is $v_{\text{free}} \cdot \Delta t$. [1] The cells in the

[1] In the MPC, it is assumed that the values of model parameters are the same for every vehicle group, so the vehicle group index, j, is omitted in the following contents for better readability.

"virtual freeway" are numbered from 0 to $-(Tp-1)$ from downstream to upstream. The traffic density of cell $-k$ on the "virtual-freeway" is calculated as,

$$\rho_{-k}\left(t\right)=\frac{d(t+k)}{v^{\text{free}}},\ 0\leqslant k<T_{\text{p}} \tag{11}$$

It is assumed that all vehicles on both the target freeway and the "virtual freeway" are uniformly distributed. Therefore, the position of a vehicle can be readily obtained if the cell that the vehicle is locating on and the density of that cell are known. The same as the model formulation presented in Section 2.1, all vehicles are formed into vehicle groups from downstream to upstream, and the position of vehicle group $j, x_j(t)$, represents the position of the most upstream vehicle in this vehicle group.

The traffic state of a vehicle group is represented by its average spacing, as defined in Eq. (2). In the MPC, the traffic dynamics can be represented by the following equation,

$$S(t+1)=S(t)+BV(t), \tag{12}$$

where

$$S(t)=\begin{bmatrix}s_1(t)\\ s_2(t)\\ \vdots\\ s_J(t)\end{bmatrix},\quad V(t)=\begin{bmatrix}v_1(t)\\ v_2(t)\\ \vdots\\ v_J(t)\end{bmatrix},\quad B=\begin{bmatrix}0 & & & & \\ \frac{\Delta t}{\Delta n} & -\frac{\Delta t}{\Delta n} & & & \\ & \frac{\Delta t}{\Delta n} & -\frac{\Delta t}{\Delta n} & & \\ & & \ddots & \ddots & \\ & & & \frac{\Delta t}{\Delta n} & -\frac{\Delta t}{\Delta n}\end{bmatrix}, \tag{13}$$

and J is the total number of vehicle groups. The prediction of traffic states over a horizon T_{p} is represented by the following equation,

$$\underline{S}\left(t\right)=AS\left(t\right)+B_1\underline{V}\left(t\right), \tag{14}$$

where

$$\underline{S}(t)=\begin{bmatrix}S(t+1)\\ S(t+2)\\ \vdots\\ S(t+T_{\text{p}})\end{bmatrix},\quad A=\begin{bmatrix}I_J\\ I_J\\ \vdots\\ I_J\end{bmatrix},\quad \underline{V}(t)=\begin{bmatrix}V(t)\\ V(t+1)\\ \vdots\\ V(t+T_{\text{p}}-1)\end{bmatrix},\quad B_1=\begin{bmatrix}B & 0 & \cdots & 0\\ B & B & & \vdots\\ \vdots & & \ddots & \\ B & B & \cdots & B\end{bmatrix}, \tag{15}$$

and I_J is the identity matrix. The average speeds of all the vehicle groups are the decision variables. The calculation of group j's speed at a future step $k, v_j(t+k)$, is delegated to the controller, and only upper bounds are specified to $v_j(t+k)$ as follows:

$$0\leqslant v_j\left(t+k\right)\leqslant v^{\text{free}},\ \forall\ 1<j\leqslant J,\ \forall\ 0\leqslant k<T_{\text{p}} \tag{16}$$

$$v_j\left(t+k\right)\leqslant\alpha\left(s_j\left(t+k\right)-s^{\text{jam}}\right),\ \forall\ 1<j\leqslant J,\ \forall\ 0\leqslant k<T_{\text{p}} \tag{17}$$

$$v_j\left(t+k\right)\leqslant\left(1-\frac{\beta}{\alpha}\right)\cdot v_j\left(t+k-1\right)+\beta\cdot\left(s_j\left(t+k\right)-s^{\text{jam}}\right),\ \forall\ 1<j\leqslant J,\ \forall\ 0\leqslant k<T_{\text{p}} \tag{18}$$

The above constraints correspond to the first three terms in Eq. (10). The black lines and the red dashed line in Fig. 1 (b) represent the upper bounds of $v_j(t+k)$, corresponding to different values of $s_j(t+k)$. In case no control actions are applied, the actual speed is equal to the minimum of the first three terms in Eq. 10 and the solution of $v_j(t+k)$ lies on the lines of the upper bounds. If the solution of $v_j(t+k)$ lies beneath the upper bounds, then vehicle group j at time step $t+k$ is under VSL control, and the solution is the optimal value of speed limit.

3.3. Objective function and constraints

The objective function of the MPC is designed as the maximization of M, which is the total travel distance (TTD) of all vehicles on both the target freeway and the downstream of the target freeway over the entire prediction horizon:

$$M=\sum_{j=1}^{J}\sum_{k=t_j^{\text{arrive}}}^{T_{\text{p}}-1}v_j\left(t+k\right)\cdot\Delta t \tag{19}$$

where t_j^{arrive} denotes the time index that vehicle group j arrives to the target freeway,

$$t_j^{\text{arrive}} = \begin{cases} 0, & \text{if } x_j(t) \geqslant 0 \\ \left\lfloor \dfrac{-x_j(t)}{v_f} \right\rfloor, & \text{if } x_j(t) < 0 \end{cases} \tag{20}$$

It is assumed that every vehicle group arrives at the target freeway at a fixed time, so the flows at the upstream boundary of the target freeway will be the same as the predicted demand. Therefore, the following constraint is imposed to the vehicle groups locating on the "virtual freeway" at time t,

$$v_j\left(t+k\right) = v^{\text{free}}, \text{ if } x_j\left(t\right) < 0 \text{ and } 0 \leqslant k \leqslant t_j^{\text{arrive}}. \tag{21}$$

Note that this constraint is not in conflict with constraints Eqs. (16)–(18), because Eq. (16) is dominating in determining the speeds of vehicle groups on the "virtual freeway" and Eq. (16) and Eq. (21) have a common solution, which is $v_j(t+k) = v^{\text{free}}$. To explain the physical meaning of M, we consider M as the summation of two terms, $M = M_1 + M_2$. A graphical interpretation of the two terms are shown in Fig. 5. The first term, M_1, denotes the total travel distance of all vehicles on the target freeway stretch and the second term, M_2, represents the total travel distance at the downstream of the target freeway stretch. The interpretation of M_2 is explained by the following proposition.

Proposition 1. Maximizing M_2 is equivalent to minimizing the total time spent (TTS) of the target freeway.

Proof. Let $q(t+k)$ represents the predicted outflow of the target freeway, then the total travel distance at the downstream of the freeway stretch, M_2, can be reformulated as:

$$M_2 = \sum_{k=0}^{T_{\text{p}}-1} q\left(t+k\right) \cdot \Delta t \cdot \left(T_{\text{p}} - k\right) \cdot v^{\text{free}}. \tag{22}$$

The TTS of the target freeway stretch is calculated as:

$$\text{TTS} = T_{\text{p}} \cdot \sum_{i=1}^{I} \rho_i\left(t\right) l_i + \sum_{k=0}^{T_{\text{p}}-1} \Delta t \cdot \left(T_{\text{p}} - k\right) \cdot (d(t+k) - q(t+k)). \tag{23}$$

Maximizing M_2 is equivalent to maximizing the term $\sum_{k=0}^{T_{\text{p}}-1}(T_{\text{p}}-k)\cdot\Delta t\cdot q(t+k)$ in Eq. (22), as v^{free} has a constant value. Minimizing the TTS is also equivalent to maximize the term $\sum_{k=0}^{T_{\text{p}}-1}(T_{\text{p}}-k)\cdot\Delta t\cdot q(t+k)$ in Eq. (23) as the terms $T_{\text{p}}\cdot\sum_{i=1}^{I}\rho_i(t)L_i$ and $\sum_{k=0}^{T_{\text{p}}-1}\Delta t\cdot(T_{\text{p}}-k)\cdot d(t+k)$ are constant. Therefore, maximizing M_2 is equivalent to minimizing the TTS of the target freeway.

As maximizing M_1 represents the maximization of TTD and maximizing M_2 is equivalent to minimizing the TTS, the objective of the proposed MPC is a weighted sum of the TTS minimization and TTD maximization. Note that this optimization does not suffer from the so-called holding back problem. Holding back may occur for a congested state, where the VSLs cannot have any influence. In Han et al. (2017b), the holding back problem was addressed by a linear quadratic objective function, where the quadratic term minimizes the quadratic function of the number of vehicles in the networks and the linear term aims to maximize the flows (Papageorgiou, 1995). In the objective function of the MPC in this paper, the term M_2 minimizes the TTS and the term M_1 pushes vehicles moving forward to address the holding back.

Typical real-world speed limit systems have some pre-defined minimum speed that can be displayed. Moreover, for safety reasons, normally the VSL variation between neighboring cells should be lower than a certain value. To this end, we impose safety constraints directly to the decision variables as follows,

$$v_j\left(t+k\right) \geqslant V^{\min}, \ \forall\ 1 < j \leqslant J, \ \forall\ t_j^{\text{arrive}} < k < T_{\text{p}}, \text{ if } \widehat{v}_j\left(t+k\right) \geqslant V^{\min} \tag{24}$$

$$v_j\left(t+k-1\right) - v_j\left(t+k\right) \leqslant \Delta V_1, \ \forall\ 1 < j \leqslant J, \ \forall\ t_j^{\text{arrive}} < k < T_{\text{p}}, \text{ if } \widehat{v}_j\left(t+k-1\right) - \widehat{v}_j\left(t+k\right) \leqslant \Delta V_1 \tag{25}$$

$$v_{j-1}\left(t+k\right) - v_j\left(t+k\right) \leqslant \Delta V_2, \ \forall\ 1 < j \leqslant J, \ \forall\ t_j^{\text{arrive}} < k < T_{\text{p}}, \text{ if } \widehat{v}_{j-1}\left(t+k\right) - \widehat{v}_j\left(t+k\right) \leqslant \Delta V_2 \tag{26}$$

where $V^{\min}$ is the minimum speed that can be displayed. ΔV_1 is the maximum speed change of a vehicle group in two consecutive time steps. ΔV_2 is the maximum speed difference of the following vehicle group and the leading vehicle group for two neighbouring vehicle groups at a time step. $\widehat{v}_j(t+k)$ is the predicted speed without VSL control. The added conditions in the above constraints are aimed to avoid the infeasibility of the optimization caused by conflicting constraints. If a safety constraint conflicts with the model constraints, i.e., Eqs. (16)–(18), the optimization model may become infeasible. Therefore, before running the optimization at each control step, the traffic states are predicted by the prediction model of the controller by running a forward simulation. It can be guaranteed that the optimization problem with the above constraints has a solution, because $\widehat{v}_j(t+k)$ is a feasible solution of the optimization problem with

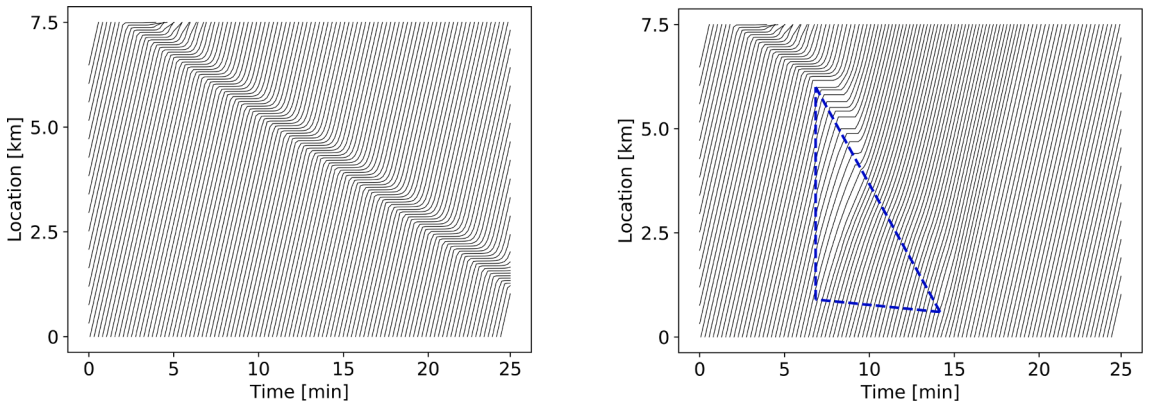

Fig. 6. The left figure is the trajectories of all vehicle groups without VSL control, and the right figure is the trajectories of all vehicle groups controlled by the proposed MPC. The VSL control area is enclosed by the blue lines.

the above constraints. Note, however, that in this way, it cannot be ensured that every $\hat{v}_j(t+k)$ under VSL control is restricted by the safety constraints. For speeds in the prediction that do not satisfy with the conditions in the above constraints, the safety constraints cannot be guaranteed. Those speeds, if exist, will be truncated to the closest feasible speed limit value before being implemented.

The overall optimization problem is formulated as:

$$\min_{\underline{V}\left(t\right)} M = \sum_{j=1}^{J} \sum_{k=t_j^{\text{arrive}}}^{T_{\text{p}}-1} v_j\left(t+k\right) \cdot \Delta t \tag{27}$$

subjectto

$$Eq.(12) - Eq.(18), Eq.(20) - Eq.(21), Eq.(24) - Eq.(26)$$

The optimization is formulated as a linear programming problem, and it can be solved by an appropriate solver (e.g., GUROBI). After the optimization at each control step, the optimal speeds can be displayed to all the drivers via in-car devices. If only roadside VSL gantries are available on a freeway, the optimal speed of a roadway segment will be calculated as the average of all the vehicle's optimal speed, which are locating on that segment.

3.4. Numerical experiment

In this subsection, we demonstrate the effectiveness of the presented MPC controller by a numerical experiment. The presented MPC is applied to the same case as in Section 2.3. The presented traffic flow model is used as both the process model and the prediction model. The prediction horizon is set to 1200s, so $T_{\text{P}} = 120$. T_{c} is set to the same value as T_{P}. T_{k} is the same as the duration of a simulation step, which is 10s. $V^{\min}$ is set to 16 m/s. ΔV_1 and ΔV_2 are set to 3 m/s per control step. The MPC controller is activated at min.7 when the jam wave has formed.

The plots of the trajectories of all vehicle groups before and after VSL control are shown in Fig. 6. The MPC controller generates a VSL control scheme that successfully resolve the jam wave. The VSL control area is enclosed by the blue lines. When the controller was activated, the flow arriving in the jam wave was reduced by VSLs, as shown by the sparser vehicle trajectories at the upstream of the jam wave. As a result of the implemented safety constraints, the speeds of the vehicles under VSLs were higher than the minimum value, i.e., 16 m/s, and there was no sharp deceleration in the speed limit area. After the jam wave was resolved, the throughput of the freeway stretch increased, as shown by the denser vehicle trajectories at the downstream of the VSL control area. Quantitatively, the total time spent saving the proposed MPC is 21.2%.

To test the robustness of the proposed controller against prediction errors, we set the demand and parameters of the prediction model to random values. Each of the four parameters ($v^{\text{free}}, s^{\text{jam}}, s^{\text{cri}}$, and $s^{\max}$) is assumed to follow a Gaussian distribution, where the mean is equal to the value of the process model and the standard deviation is 2% of the mean. The demand is also assumed to follow a Gaussian distribution, where the mean is equal to 5500 veh/h and the standard deviation is 5% of the mean. The MPC controller is tested for 10 times, applying the presented demand and parameter settings. The total time spend savings are in the range of 16.6%-18.9%.

4. The hierarchical VSL control with CAVs

In this section, we extend the proposed MPC to a hierarchical VSL control approach which includes two levels. At the upper level, the proposed discrete MPC-VSL calculates the optimal speed limit of each vehicle group. At the lower level, we apply continuous MPC to optimize the trajectories of several randomly distributed CAVs followed by human-driven vehicles, such that the optimal speeds

from the upper level can be realized using CAVs as distributed traffic control actuators.

4.1. System architecture

Although V2V based CAVs can increase roadway capacity and flow stability, at low market penetration rates traffic control layer is still essential to mitigate congestion (Roncoli et al., 2015; Wang et al., 2016). Motivated by designing a system that leverages the potential of CAVs at very low market penetration rates, the proposed MPC of VSLs is integrated into a hierarchical framework using CAVs randomly distributed in traffic as actuators of VSL control.

The presented MPC in the previous section decides the optimal target speed of each vehicle group at the upper macroscopic level with a prediction horizon of around 20 min. At the lower microscopic level, all the vehicles are regrouped such that the leaders of the platoons are CAVs, which are regarded as actuators of the upper layer. Acceleration trajectories of CAVs are optimized under continuous MPC in a short horizon of in the order of 5–10 s at so that the human-driven vehicles following them reach the target speed assigned by the traffic control layer efficiently and smoothly while ensuring collision-free with the predecessor.

4.2. System dynamics model

Following the notation tradition of the previous section, we use capital to denote state and control variables at the vehicle level, while we add a superscript (mic) to denote the position, speed at the *microscopic vehicle level*.

The system state from the perspective of a connected optimal car-following control (CO-CFC) vehicle $\imath$ can be described by $X = (s_\imath^{\mathrm{mic}}, v_\imath^{\mathrm{mic}})^T$. $s_\imath^{\mathrm{mic}}$ denotes the (distance) gap to the preceding vehicle $\imath-1$, i.e. $s_\imath^{\mathrm{mic}} = x_{\imath-1}^{\mathrm{mic}} - x_\imath^{\mathrm{mic}} - l_\imath^{\mathrm{mic}}$, with $l_\imath^{\mathrm{mic}}$ representing the vehicle length. Note as we discussed in Section 4.1, the lower VSL layer treat the CO-CFC vehicle $\imath$ as the platoon leader. Hence the position of its preceding vehicle $\imath-1$ is actually the position of the downstream platoon preceding the platoon the CO-CFC is leading.

The state variables can be directly measured from onboard sensors of CO-CFC vehicles, e.g. radar. The longitudinal dynamics model of the system used for predicting future evolution of the system is described by the following differential equation:

$$\frac{d}{dt}X = \frac{d}{dt}\begin{pmatrix} s_\imath^{\mathrm{mic}} \\ v_\imath^{\mathrm{mic}} \end{pmatrix} = \begin{pmatrix} v_{\imath-1}^{\mathrm{mic}} - v_\imath^{\mathrm{mic}} \\ u_\imath^{\mathrm{mic}} \end{pmatrix} = \begin{pmatrix} \Delta v_\imath^{\mathrm{mic}} \\ u_\imath^{\mathrm{mic}} \end{pmatrix} = \mathbf{f}\left(X, U, D\right) \tag{28}$$

$\Delta v_\imath^{\mathrm{mic}} = v_{\imath-1}^{\mathrm{mic}} - v_\imath^{\mathrm{mic}}$ denotes relative speed to the preceding vehicle. $U = u_\imath^{\mathrm{mic}}$ is the acceleration of CO-CFC vehicle $\imath$.

Here, $D = v_{\imath-1}^{\mathrm{mic}}$ denotes the exogenous disturbance, which is the preceding vehicle speed. The disturbance can be modelled by using *constant speed heuristics* (Wang et al., 2015), i.e. the predecessor travels at the measured speed in the predicted future. In the closed-loop system, the preceding vehicle is not necessarily travelling at constant speed. The predecessor speed variation is the source of the mismatch between the open-loop prediction model and the closed-loop system behaviour.

The CO-CFC controller should cope with the mismatch between the model and the system and generate locally stable behaviour. As we will show with simulation in the ensuing, the CO-CFC controller is quite robust to the mismatch due to the feedback nature of the receding horizon process.

4.3. Optimal acceleration control under speed limits

At each time t_0, the CO-CFC system seeks an optimal control trajectory $U(\cdot)$ in the finite prediction horizon $[t_0, t_0+H_p)$ that minimizes a cost function $\mathscr{V}$ (Mayne, 2014). It can be formulated as the following mathematical programme:

$$\min_{U_{[t_0,t_0+H_p)}} \mathscr{V}\left(X\left(t\right), U\left(t\right)\right) = \min_{U_{[t_0,t_0+H_p)}} \left(\int_{t_0}^{t_0+H_P} \mathscr{L}(X(t), U(t), D(t))dt + \mathscr{G}\left(X\left(t_0+H_p\right)\right) \right) \tag{29}$$

where $\mathscr{V}$ denotes the cost function to be minimized. $\mathscr{L}$ denotes the so-called running cost and $\mathscr{G}$ denotes the so-called terminal cost. The terminal cost is chosen to be zero to ensure closed-loop stability of the MPC controller (Mayne et al., 2000; Duret et al., 2020).

The optimization is subject to:

- the system dynamics model of Eq. (28)
- the initial condition:

$$X(t_0) = X_0 \tag{30}$$

- the constraints on state and control variables:

$$X(t) \in \mathscr{X}, U(t) \in \mathscr{U} \tag{31}$$

The running cost function is defined as:

$$\mathscr{L} = \underbrace{\frac{c_1}{s_\iota^{\mathrm{mic}}}\left(\Delta v_\iota^{\mathrm{mic}}\right)^2}_{\text{safety}} + \underbrace{c_2\left(v^d\left(s_\iota^{\mathrm{mic}}\right) - v_\iota^{\mathrm{mic}}\right)^2}_{\text{efficiency}} + \underbrace{c_3\left(u_\iota^{\mathrm{mic}}\right)^2}_{\text{control}} \tag{32}$$

In Eq. (32), the *safety* cost term guarantees that the CO-CFC vehicle will get a large penalty when approaching the preceding vehicle at small gaps, since these situations entail high risks of rear-end collisions. When there is no preceding vehicle detected by the on-board sensor, the safety cost term vanishes.

The safety cost is the proximity cost terms reflecting the interaction with the preceding vehicle. The *efficiency* cost implies that the vehicle tends to track the desired speed determined by the speed limits and the distance to the predecessor. Specifically, the desired speed v^d is determined by:

$$v^d\left(s_\iota^{\mathrm{mic}}\right) = \min\left\{v_\iota^{\mathrm{VSL}}, \frac{s_\iota^{\mathrm{mic}} - s_0^{\mathrm{mic}}}{t^d}\right\} \tag{33}$$

v_ι^{VSL} is the target variable speed limits *commanded by the upper VSL layer*. This is the *macroscopic average speed of the group vehicle* ι *is leading*. t^d denotes the user-defined desired time gap. s_0^{mic} denotes the minimum distance. When speed limits are activated, the v_ι^{VSL} is dominating the desired speed of vehicle ι, incurring a high cost of deviating from the desired speed and pushing the CO-CFC to track the commanded speed from the upper VSL layer.

The control cost is represented by penalizing acceleration or deceleration. It ensures the resulting optimal trajectory of the controlled vehicle is smooth, so do the human-driven vehicles following them. This is particularly important under dynamic VSL. Since large accelerations and decelerations also reflect discomfort, this cost can also be interpreted as comfort cost.

The constraint on the state variable $\mathscr{X}$ is specified as:

$$\mathscr{X} := \left\{s_\iota^{\mathrm{mic}} > s_0; v_\iota^{\mathrm{mic}} \in \left[0, v_{\max}\right]\right\} \tag{34}$$

The constraint implies that the gap with respect to the preceding vehicle should be no less than the minimum distance s_0^{mic} and the controlled vehicle drives within a speed range of $[0, v_{\max}]$. The controlled inputs are limited to some admissible bounds:

$$\mathscr{U} := \left\{u_\iota^{\mathrm{mic}} \in \left[a_{\min}, a_{\max}\right]\right\} \tag{35}$$

4.4. Derivation of optimal acceleration

This section shows how to solve the optimal control problem based on Pontrygain's Principle (Pontryagin et al., 1962; Wang et al., 2012). Without going too much into details, the solution approach entails defining the Hamiltonian $\mathscr{H}$ as follows:

$$\mathscr{H}\left(X, U, \Lambda\right) = \mathscr{L}\left(X, U, D\right) + \Lambda^T \cdot \mathbf{f}\left(X, U, D\right) \tag{36}$$

where $\Lambda = (\lambda^s, \lambda^v)^T$ denotes the so-called *co-state* or *marginal cost* of the state X, which reflects the relative extra cost of $\mathscr{V}$ incurred due to making a small change δX on the state X.

Using the Hamiltonian, we can derive the following necessary condition for the optimal control $\mathbf{u}^*$:

$$U^* = \min \mathscr{H}(X, U, \Lambda), \text{s.t.} U \in \mathscr{U}, X \in \mathscr{X} \tag{37}$$

Eq. (37) shows that the optimal control $\mathbf{u}^*$ minimizes the Hamiltonian in the admissible range $\mathscr{U}$ and in the bounded set $\mathscr{X}$. This requirement will enable expressing the optimal control input U^* as a function of the state X and the co-state Λ:

$$U^* = \frac{-\lambda^v}{2c_3} \tag{38}$$

The co-state are derived as:

$$-\frac{d\lambda^s}{dt} = \frac{\partial \mathscr{H}}{\partial s_\iota^{\mathrm{mic}}} = -\frac{c_1}{\left(s_\iota^{\mathrm{mic}}\right)^2}\left(\Delta v_\iota^{\mathrm{mic}}\right)^2 + \frac{2c_2}{t_d}\left(v^d\left(s_\iota^{\mathrm{mic}}\right) - v_\iota^{\mathrm{mic}}\right) \tag{39}$$

$$-\frac{d\lambda^v}{dt} = \frac{\partial \mathscr{H}}{\partial v_\iota^{\mathrm{mic}}} = -\frac{2c_1}{s_\iota^{\mathrm{mic}}}\Delta v_\iota^{\mathrm{mic}} - 2c_2\left(v^d\left(s_\iota^{\mathrm{mic}}\right) - v_\iota^{\mathrm{mic}}\right) - \lambda^s \tag{40}$$

The state dynamics Eq. (28) and the co-state dynamics equation of (39, 40) constitute a set of ordinary differential equations with initial conditions and terminal conditions. An iterative numerical solution algorithm will be used to solve the two-point boundary value problem efficiently (Wang et al., 2015).

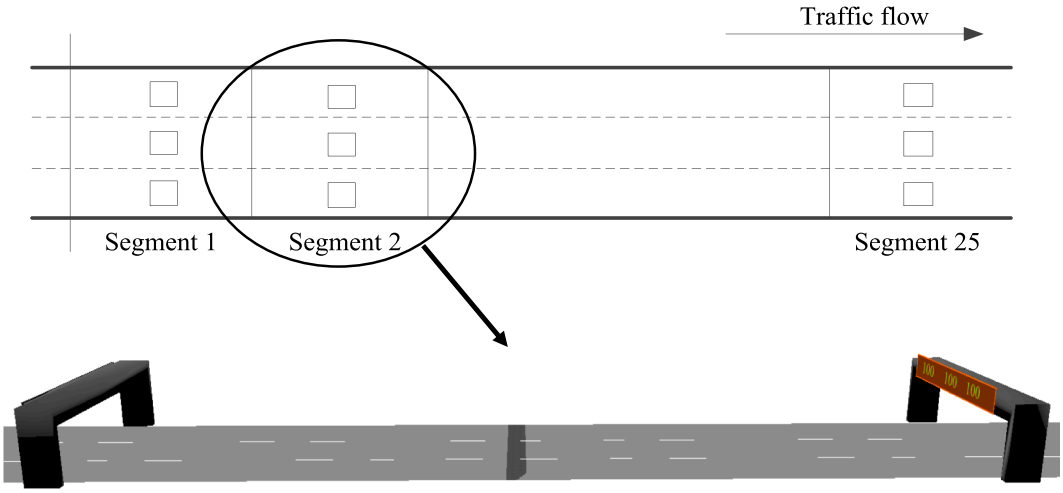

Fig. 7. The sketch of the synthetic freeway in the simulation experiment.

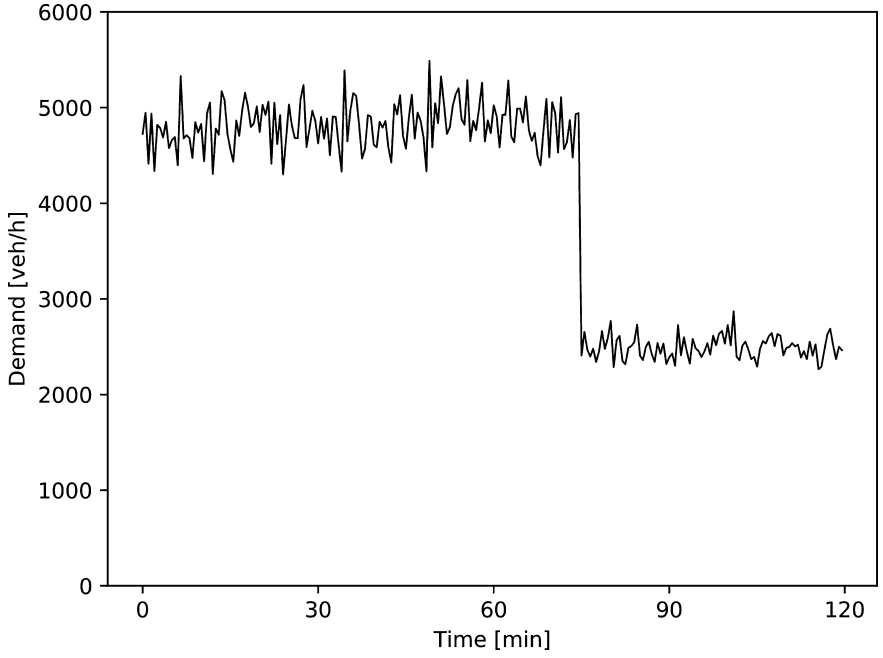

Fig. 8. The demand profile of the simulation.

5. Simulation experiments

In this section, we test the effectiveness of the presented MPC approach and the hierarchical VSL control approach in microscopic simulation environments. The MPC approach is tested in the microscopic traffic simulator VISSIM for conventional traffic with 100% human-driven vehicles. The hierarchical MPC based VSL and CO-CFC control are tested in a single-lane simulator where human drivers are modelled with the improved version of intelligent driving model, IDM+ (Schakel et al., 2012). This can avoid black-box behavior modules when implementing CAV acceleration control algorithms in a commercial simulation software.

5.1. Testing the MPC approach

The presented MPC control approach is implemented in Python and integrated into VISSIM through the COM interface. To mimic the potential field implementation locations (e.g., Rongwu freeway in China) of the presented approach, we build a synthetic three-lane freeway stretch of 7.5 km in length according to the freeway design. Variable speed limit signs are placed every 300 m along the

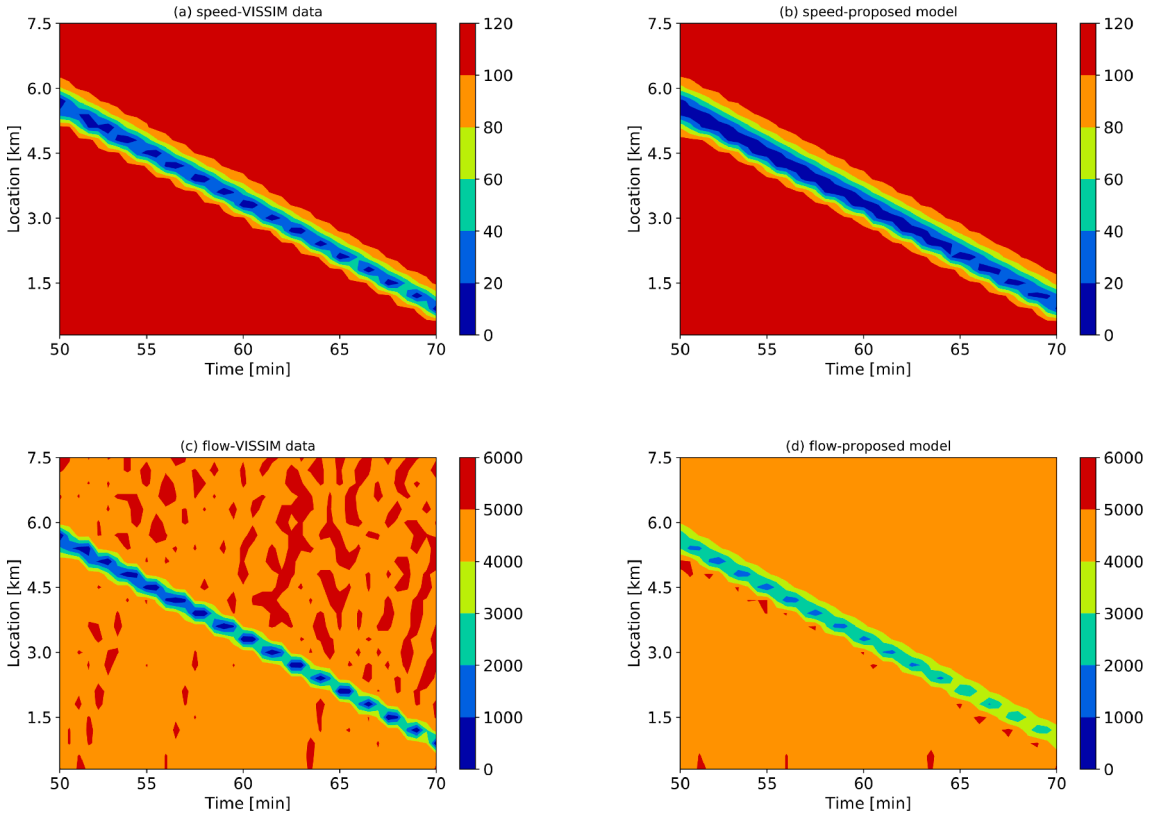

Fig. 9. The comparison between the original and the reproduced speed and flow contour plots.

freeway, which divides the freeway stretch into 25 segments. Loop detectors are placed in the middle of every segment, measuring speed, occupancy, and traffic counts every 30s. A graphical representation of the synthetic freeway is shown in Fig. 7. The model parameters in VISSIM are referred to Hegyi et al. (2013), in which the SPECIALIST algorithm was tested for jam waves suppression.

The entire traffic simulation process is 2 h, including 1.5 peak hours and 0.5 off-peak hours. Traffic demands are set to 1600 veh/h/lane on average for peak hours and 800 veh/h/lane for off-peak hours, and a Gaussian noise (the standard deviation is 5% of the average value) is added to mimic traffic demand fluctuations in reality. The demand profile of the simulation is shown in Fig. 8. To create a jam wave, we artificially close two lanes in the period 480-600s (40–42 min) at the downstream boundary of the freeway stretch. The speed and flow contour plots of the jam wave simulation are shown as Fig. 10(a) and (c). The free-flow capacity in the simulation is around 2000 veh/h/lane, and the queue discharge rate is about 1600 veh/h/lane, leading to a capacity drop of 20%.

The presented model is calibrated using traffic flow data from the simulation. The parameter calibration problem is formulated as a non-linear optimization problem which aims to minimize the discrepancy between the model predictions and the real data. The following formula is used to represent the performance indicator H,

$$H = \min \varphi^q \sqrt{\frac{\sum_{t=t_1}^{t_2}\sum_{i=1}^{I}\left[q_i(t)-\widetilde{q}_i(t)\right]^2}{I\cdot(t_2-t_1)}} + \varphi^v \sqrt{\frac{\sum_{t=t_1}^{t_2}\sum_{i=1}^{I}\left[v_i(t)-\widetilde{v}_i(t)\right]^2}{I\cdot(t_2-t_1)}}, \tag{41}$$

where, $q_i(t)$ and $v_i(t)$ are the flow and speed calculated by the model at segment i. $\widetilde{q}_i(t)$ and $\widetilde{v}_i(t)$ are the flows and speeds measured in the simulation. φ^q and φ^v are set to values $\overline{q}^{-1}$ and $\overline{v}^{-1}$ respectively to normalize the results, where $\overline{q}$ and $\overline{v}$ are the average measured flow and speed. The Nelder-Mead algorithm (Lagarias et al., 1998; Nelder and Mead, 1965), which has been demonstrated as an effective method for macroscopic traffic flow model calibration (Spiliopoulou et al., 2017), is employed as the solution algorithm for the optimization. To ensure that a global optimum is achieved, multiple starting points which are based on empirical initial guess and random noises are used.

The calibrated parameters are listed as follows: v^{free} is 29.94 m/s. s^{jam},s^{cri}, and $s^{\max}$ are 7.65 m, 54.93 m, and 85.40 m, respectively. Fig. 9 shows the comparison between the original simulated and the model reproduced speed and flow contour plots. In general, the jam wave size, magnitude and propagation speed reproduced from the Lagrangian model agree well with simulated data. The flow error and the speed error of the presented model are 8.6 % and 9.1 %. As a comparison, we calibrate a discrete Eulerian LWR model, which has also been developed into an optimal VSL controller in (Han et al., 2017b). The flow error and the speed error form the Eulerian LWR model are 17.9 % and 18.3 % respectively, which are much higher than the presented Lagrangian model.

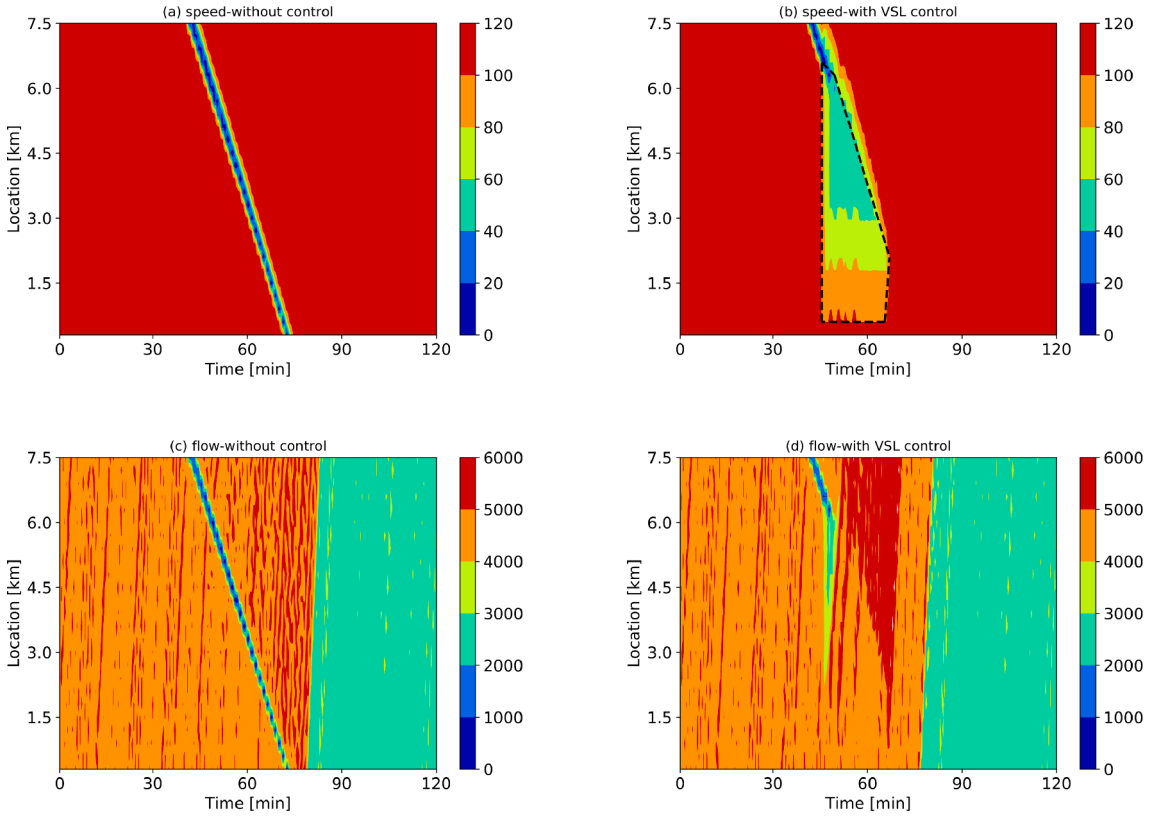

Fig. 10. (a) and (c) are the simulated (in VISSIM) speed [km/h] and flow [veh/h] contour plots without VSL control. (b) and (d) are the speed and flow contour plots with the MPC controller implemented.

The presented MPC controller is implemented to the simulation to suppress the jam wave. To tune the parameters of T_p and T_c, we follow the rule that T_p should be larger than the typical travel time from the controlled segments to the exit of the network, and T_c should has a good trade-off between the computational effort and the performance. The prediction horizon and control horizon are set to 20 min, and the duration of a control step T_k is set to 30 s. V^{min} is set to 16 m/s. ΔV_1 and ΔV_2 are set to 3 m/s per control step. After each optimization run, the obtained optimal speed of every segment is rounded to the closest value in multiples of 5 km/h, such that it can be display via a variable message sign. The controllers are assumed to be activated at minute 45 when the jam wave has formed and deactivated if the speed of every segment is higher than 70 km/h so there will be little risk to form a new jam. The non-compliance factor θ is set to 0, so the drivers are assumed to fully comply with the displayed speed limits. Note this full compliance is only used for prediction in MPC. In VISSIM simulation representing the real system, drivers choose their own desired speed according to the displayed speed limits and hence they may not comply with the displayed speed limits.

Traffic performance of the proposed MPC controller is depicted in Fig. 10. From Fig. 10 (b) it can be seen that the jam wave is successfully resolved by the MPC controller. Inside the black dashed lines is the VSL control area. It also can be seen that safety constraints are reasonably implemented in the MPC, as there is no sharp speed reduction in the speed limit area. The comparison between Fig. 10 (c) and (d) shows that the flows at the downstream of the VSL-controlled area are significantly higher than the counterpart (flows at the downstream of the jam wave) in the scenario without VSL control. Quantitatively, the total time spent(TTS) in the time period 45–75 min of the scenario without VSL control is 231.6 h. The TTS of the control scenario in the same time period 215.8 h, which is 7.3 % lower than the scenario without VSL control. Moreover, since the jam wave is not resolved in the scenario without VSL control, the jam will propagate further upstream and can activate or worsen upstream bottlenecks.

A computer with an I7-8565U processor and 16 GB RAM is used for the optimizations. The computation time for the optimizations are between 4s and 11s, which is fast enough for an online application. For the sake of compactness, we omit the comparison of the proposed controller with other MPC controllers. In our previous work, we have tested and compared three other MPC controllers (including both linear and nonlinear MPCs) of VSLs in a similar test-bed (Han et al., 2017b). In that paper, a linear quadratic MPC based on an extended discrete LWR model formulated in Eulerian coordinate was proposed, and it was demonstrated to achieve a good performance in reducing total travel delay and maintaining a low computation time. As the prediction model of the proposed MPC is shown to be more accurate than the prediction model in our previous MPC, and the optimization of proposed MPC is more flexible for adding VSLs constraints, we consider the proposed MPC is more advanced than our previous MPC. For the details of the comparison, readers are referred to (Han et al., 2017b).

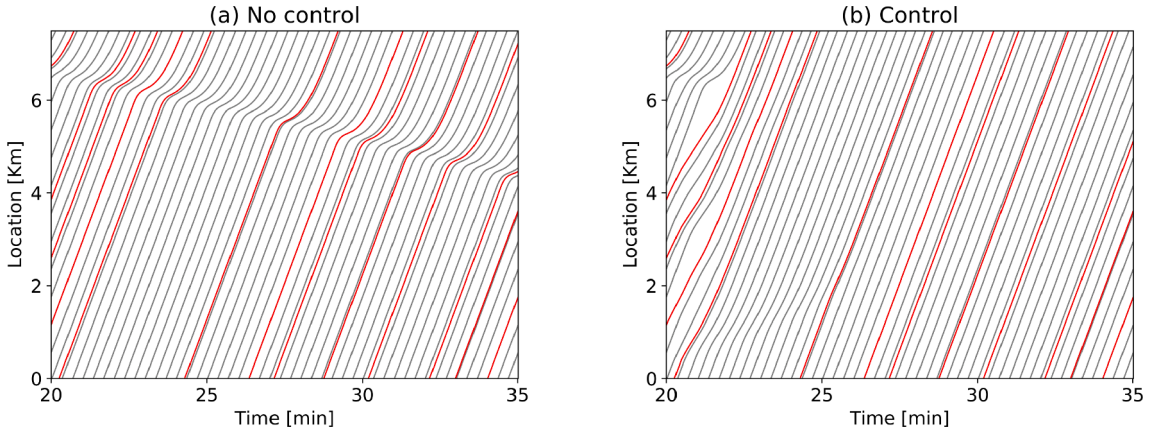

Fig. 11. (a) and (b) are sample trajectories (during min. 20–35) from the no control case and a control case. CAVs trajectories are depicted in red. One out of every ten human-driven vehicles' trajectory are selected and depicted in gray.

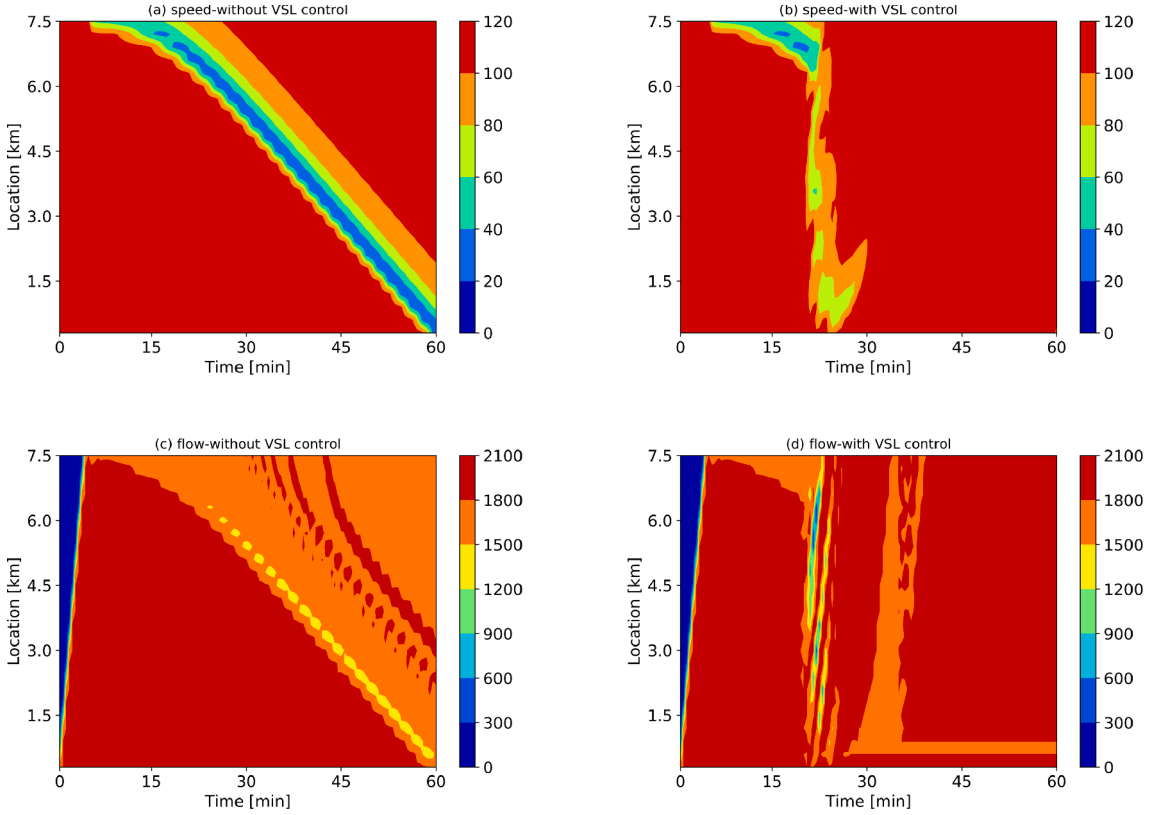

Fig. 12. (a) and (c) are the simulated (by IDM+) speed [km/h] and flow [veh/h] contour plots without VSL control. (b) and (d) are the speed and flow contour plots with the hierarchical VSL control approach implemented.

5.2. Testing the hierarchical control approach

In this subsection, we test the presented hierarchical VSL control approach using the IDM + model as the process model, which is implemented in MATLAB. The testing network is a 7.5 km single-lane freeway stretch. It is assumed that all vehicles on the freeway are connected vehicles and their positions and speeds can be obtained in real time. 5% of the connected vehicles are automated vehicles equipped with CO-CFC system randomly distributed in the traffic, so their acceleration and deceleration can be adjusted in real time. The rest 95% are human-driven vehicles that do not receive VSL information so their desired speeds remain as free flow speed.

The simulation lasts for one hour, and traffic demand of the entire simulation period is set to 1800 veh/h constantly. To create a jam

wave, an artificial disruption is created. The desired speed of all drivers is reduced in the period 150–300s to 40 km/h on the location of 7200–7500 m. The simulated speed and flow contour plots are shown in Fig. 12 (a) and (c). The TTS is 139.2 h for the uncontrolled case. Parameters of the upper level controller are set to the same values as that in the previous subsection. $T_p = T_c = 20$ minutes, and $T_k = 30$ s. As the lower level controller has considered the safety of vehicles inherently, all the safety constraints in the upper level controller are relaxed. The prediction model in the upper level controller is calibrated using the same approach as that in the previous subsection, and the calibrated values of model parameters are: $v^{free} = 29.61$ m/s, $s^{jam} = 6.34$ m, $s^{cri} = 55.70$ m, and $s^{max} = 69.53$ m. The CO-CFC controller parameters are set as: $H_p = 5$ s, $c_1 = 10$, $c_2 = 0.05$, $c_3 = 0.5$, $t_d = 1.3$, $s_0^{mic} = 2$ m. The lower MPC is recalculated at a resolution of 0.5 s. Parameters of IDM + can be found in Schakel et al., 2012.

The controller is activated at time 1200s, when the jam wave has already formed, and deactivated if all the vehicles are driving at a speed higher than 60 km/h. To test if the presented control approach is influenced by the distribution of the CO-CFC vehicles, the control approach is ran for multiple times, using the same input (demand, boundary conditions, and values of parameters) but different (random) distribution of the CO-CFC vehicles. The results show that the presented control approach is not sensitive to the random distribution of the CO-CFC vehicles. In 10 simulation tests, the TTS varies between 124.8–126.7 h, which are 9.0 % - 10.3 % lower than that without VSL control. The speed and flow contour plots of an example are shown in Fig. 12 (b) and (d). Fig. 11 shows sample trajectories of this example and the case without VSL control. In the figure, CAVs trajectories are depicted by red lines. From Fig. 11 (b) it can be observed that the deceleration of CAVs at the upstream of the jam wave enlarges the spacing between vehicles and reduces the arriving flow to the jam. This process results in the dissipation of the jam wave.

We test the hierarchical controller at different H_p and it shows similar performance. This is in line with our earlier findings that the prediction horizon does not influence the controller performance significantly as long as it is no less than 5 s Wang et al., 2015. In all the simulation tests, the human-driven vehicle trajectories are smooth since they follow CO-CFC vehicles that penalize jerky trajectories. In the 10 simulation runs, we did not observe new jams occurring due to activation and deactivation of VSL. Note also that the hierarchical approach presented here does not rely on road-based sensors (e.g. loop detectors, cameras etc.) and actuators (e.g. VSL gantries) that are expensive to install and maintain. We remark that the proposed MPC based VSL control works in a different process model with mismatch and the hierarchical approach is effective even when only 5% of the vehicles are changing their desired speed as compliance to the upper layer.

6. Findings and conclusions

This paper has presented a linear MPC of VSLs based on an extended discrete Lagrangian LWR model. The extended model keeps the linear property of the original discrete Lagrangian LWR model, and meanwhile takes capacity drop and VSLs effects into account. The optimization in the presented MPC is formulated as a linear programming problem, which can be solved efficiently. Unlike conventional discrete LWR model-based MPC of VSLs that developed based on Eulerian models with flows as decision variables, the presented MPC is able to implement safety constraints straightforward to the optimization, as the decision variables are average speed of vehicle groups. A microscopic simulation experiment has been conducted to test the performance the presented MPC, and simulation results show that the presented MPC resolves the jam wave efficiently with reasonable safety constraints implemented.

This paper has extended the presented MPC to a hierarchical VSL control framework that can be applied to a connected vehicle environment. At the upper level, the presented MPC decides the optimal speed of each vehicle group and at the lower level, the speed trajectories of some randomly distributed CO-CFC vehicles are optimized so that the human-driven vehicles following them reach the target speed from the upper layer efficiently and smoothly. The presented hierarchical VSL control approach has been tested in another microscopic environment, where the IDM + model is utilized as the process model. Simulation results show that the presented hierarchical control approach can effectively resolve jam waves in a single-lane freeway, even though the penetration rate of the CO-CFC vehicles is as low as 5%.

For future research, the hierarchical VSL control approach will be further extended, such that it can be applied to a multiple-lane freeway stretch. At current stage, lane changing is not considered by the presented approach. Furthermore, at the lower level controller, the interactions between the leading vehicle (the actuator) and the following vehicles in a platoon will be explicitly considered in the optimization, and the robustness of the controller against local disturbances will be specifically tested.

CRediT authorship contribution statement

Yu Han: Conceptualization, Methodology, Coding, Simulation development, Writing - original draft. **Meng Wang:** Methodology, Coding, Writing - original draft. **Ziang He:** Simulation development. **Zhibin Li:** Conceptualization. **Hao Wang:** Conceptualization. **Pan Liu:** Conceptualization, Supervision.

Acknowledgement

This research is jointly supported by the National Natural Science Foundation of China (No. 51925801, No.52002065), and the Natural Science Foundation of Jiangsu (No.BK20200378).

References

Carlson, R.C., Papamichail, I., Papageorgiou, M., Messmer, A., 2010. Optimal motorway traffic flow control involving variable speed limits and ramp metering. Transport. Sci. 44 (2), 238–253.

Carlson, R.C., Papamichail, I., Papageorgiou, M., 2011. Local feedback-based mainstream traffic flow control on motorways using variable speed limits. IEEE Trans. Intell. Transp. Syst. 12 (4), 1261–1276.

Chen, D., Ahn, S., 2015. Variable speed limit control for severe non-recurrent freeway bottlenecks. Transport. Res. Part C: Emerg. Technol. 51, 210–230.

Chen, D., Ahn, S., Hegyi, A., 2014. Variable speed limit control for steady and oscillatory queues at fixed freeway bottlenecks. Transport. Res. Part B: Methodol. 70, 340–358.

Courant, R., Friedrichs, K.O., 1999. Supersonic flow and shock waves,, volume 21. Springer Science & Business Media.

Daganzo, C.F., 1994. The cell transmission model: A dynamic representation of highway traffic consistent with the hydrodynamic theory. Transport. Res. Part B: Methodol. 28 (4), 269–287.

Duret, A., Wang, M., Ladino, A., 2020. A hierarchical approach for splitting truck platoons near network discontinuities. Transport. Res. Part B: Methodol. 132, 285–302.

Ghiasi, A., Li, X., Ma, J., 2019. A mixed traffic speed harmonization model with connected autonomous vehicles. Transport. Res. Part C: Emerg. Technol. 104, 210–233.

Hadiuzzaman, M., Qiu, T.Z., 2013. Cell transmission model based variable speed limit control for freeways. Can. J. Civ. Eng. 40 (1), 46–56.

Han, Y., Chen, D., Ahn, S., Hegyi, A., 2015. Analysis of driver response and traffic evolution under variable speed limit control. Transport. Res. Rec.: J. Transport. Res. Board 2490, 1–10.

Han, Y., Yuan, Y., Hegyi, A., Hoogendoorn, S.P., 2016. New extended discrete first-order model to reproduce propagation of jam waves. Transportation Research Record: Journal of the Transportation Research Board 2560, 108–118.

Han, Y., Hegyi, A., Yuan, Y., Hoogendoorn, S., 2017a. Validation of an extended discrete first-order model with variable speed limits. Transport. Res. Part C: Emerg. Technol. 83, 1–17.

Han, Y., Hegyi, A., Yuan, Y., Hoogendoorn, S., Papageorgiou, M., Roncoli, C., 2017b. Resolving freeway jam waves by discrete first-order model-based predictive control of variable speed limits. Transport. Res. Part C: Emerg. Technol. 77, 405–420.

Han, Y., Ramezani, M., Hegyi, A., Yuan, Y., Hoogendoorn, S., 2020. Hierarchical ramp metering in freeways: an aggregated modeling and control approach. Transport. Res. Part C: Emerg. Technol. 110, 1–19.

Hegyi, A. and Hoogendoorn, S. Dynamic speed limit control to resolve shock waves on freeways-field test results of the specialist algorithm. In 13th International IEEE Conference on Intelligent Transportation Systems (ITSC 2010), pages 519–524. IEEE, 2010.

Hegyi, A., Hoogendoorn, S., Schreuder, M., Stoelhorst, H., and Viti, F. Specialist: A dynamic speed limit control algorithm based on shock wave theory. In: 11th International IEEE Conference on Intelligent Transportation Systems (ITSC 2008), pages 827–832. IEEE, 2008.

Hegyi, A., De Schutter, B., Hellendoorn, H., 2005. Model predictive control for optimal coordination of ramp metering and variable speed limits. Transport. Res. Part C: Emerg. Technol. 13 (3), 185–209.

Hegyi, A., De Schutter, B., Hellendoorn, J., 2005. Optimal coordination of variable speed limits to suppress shock waves. IEEE Trans. Intell. Transp. Syst. 6 (1), 102–112.

Hegyi, A., Netten, B.D., Wang, M., Schakel, W., Schreiter, T., Yuan, Y., van Arem, B., and Alkim, T.A cooperative system based variable speed limit control algorithm against jam waves-an extension of the specialist algorithm. In 16th International IEEE Conference on Intelligent Transportation Systems (ITSC 2013), pages 973–978. IEEE, 2013.

Jin, H.-Y., Jin, W.-L., 2015. Control of a lane-drop bottleneck through variable speed limits. Transport. Res. Part C: Emerg. Technol. 58, 568–584.

Kerner, B.S., Rehborn, H., 1996. Experimental features and characteristics of traffic jams. Phys. Rev. E 53 (2), R1297.

Khondaker, B., Kattan, L., 2015. Variable speed limit: A microscopic analysis in a connected vehicle environment. Transport. Res. Part C: Emerg. Technol. 58, 146–159.

Kotsialos, A., Papageorgiou, M., Diakaki, C., Pavlis, Y., Middelham, F., 2002. Traffic flow modeling of large-scale motorway networks using the macroscopic modeling tool metanet. IEEE Trans. Intell. Transp. Syst. 3 (4), 282–292.

Lagarias, J.C., Reeds, J.A., Wright, M.H., Wright, P.E., 1998. Convergence properties of the nelder–mead simplex method in low dimensions. SIAM Journal on optimization 9 (1), 112–147.

Le, T., Vu, H.L., Nazarathy, Y., Vo, B., Hoogendoorn, S., 2013. Linear-quadratic model predictive control for urban traffic networks. Procedia-Social and Behavioral Sciences 80, 512–530.

Leclercq, L., Laval, J.A., Chevallier, E., 2007. The lagrangian coordinates and what it means for first order traffic flow models. In: 17th International Symposium on Transportation and Traffic Theory (ISTTT).

Li, Z., Liu, P., Xu, C., Duan, H., Wang, W., 2017. Reinforcement learning-based variable speed limit control strategy to reduce traffic congestion at freeway recurrent bottlenecks. IEEE transactions on intelligent transportation systems 18 (11), 3204–3217location|child::sb:host[1]/sb:edited-book/sb:publisher/sb:location)"_ $^!"boolean(child::sb:host/sb:pages)">.

Lighthill, M.J., Whitham, G.B., 1955. On kinematic waves. ii. a theory of traffic flow on long crowded roads. In Proceedings of the Royal Society of London A: Mathematical, Physical and Engineering Sciences, volume 229, pages 317–345. The Royal Society, 1955.

Liu, H., Kan, X.D., Shladover, S.E., Lu, X.-Y., Ferlis, R.E., 2018. Modeling impacts of cooperative adaptive cruise control on mixed traffic flow in multi-lane freeway facilities. Transport. Res. Part C: Emerg. Technol. 95, 261–279.

Ma, J., Li, X., Shladover, S., Rakha, H.A., Lu, X., Jagannathan, R., Dailey, D.J., 2016. Freeway speed harmonization. IEEE Transactions on Intelligent Vehicles 1 (1), 78–89.

Mahajan, N., Hegyi, A., De Weg, V., Sterk, G., and Hoogendoorn, S.P. Integrated variable speed limit and ramp metering control against jam waves–a coscal v2 based approach. In 18th International IEEE Conference on Intelligent Transportation Systems (ITSC 2015), pages 1156–1162. IEEE, 2015.

Mayne, D.Q., Rawlings, J.B., Rao, C.V., Scokaert, P.O.M., 2000. Constrained model predictive control: Stability and optimality. Automatica 36 (6), 789–814.

Mayne, D.Q., 2014. Model predictive control: Recent developments and future promise. Automatica 50 (12), 2967–2986.

Messmer, A., Papageorgiou, M., 1990. Metanet: A macroscopic simulation program for motorway networks. Traffic engineering & control 31 (9).

Muralidharan, A., Horowitz, R., 2015. Computationally efficient model predictive control of freeway networks. Transport. Res. Part C: Emerg. Technol.

Nelder, J.A., Mead, R., 1965. A simplex method for function minimization. The computer journal 7 (4), 308–313.

Papageorgiou, M., 1995. An integrated control approach for traffic corridors. Transport. Res. Part C: Emerg. Technol. 3 (1), 19–30.

Papageorgiou, M., Diakaki, C., Dinopoulou, V., Kotsialos, A., Wang, Y., 2003. Review of road traffic control strategies. Proc. IEEE 91 (12), 2043–2067.

Papageorgiou, M., Kosmatopoulos, E., Papamichail, I., 2008. Effects of variable speed limits on motorway traffic flow. Transportation Research Record: Journal of the Transportation Research Board 2047, 37–48.

Papamichail, I., Papageorgiou, M., Stamatakis, I., 2018. Feedback traffic control at highway work zones using variable speed limits. IFAC-PapersOnLine 51 (9), 329–336.

Pontryagin, L., Boltyanskij, V., Gamkrelidze, R., Mishchenko, E., 1962. The mathematical theory of optimal processes. john wiley & sons, New York.

Roncoli, C., Papageorgiou, M., Papamichail, I., 2015. Traffic flow optimisation in presence of vehicle automation and communication systems–part ii: Optimal control for multi-lane motorways. Transport. Res. Part C: Emerg. Technol. 57, 260–275.

Schakel, W.J., Knoop, V., van Arem, B., 2012. Integrated lane change model with relaxation and synchronization. Transportation Research Record: Journal of the Transportation Research Board 2316, 47–57.

Soriguera, F., Martínez, I., Sala, M., Menéndez, M., 2017. Effects of low speed limits on freeway traffic flow. Transport. Res. Part C: Emerg. Technol. 77, 257–274.

Spiliopoulou, A., Papamichail, I., Papageorgiou, M., Tyrinopoulos, Y., Chrysoulakis, J., 2017. Macroscopic traffic flow model calibration using different optimization algorithms. Oper. Res. Int. Journal 17 (1), 145–164.
Talebpour, A., Mahmassani, H.S., Hamdar, S.H., 2013. Speed harmonization: Evaluation of effectiveness under congested conditions. Transp. Res. Rec. 2391, 69–79.
Tian, J., Zhang, H., Treiber, M., Jiang, R., Gao, Z.-Y., Jia, B., 2019. On the role of speed adaptation and spacing indifference in traffic instability: Evidence from car-following experiments and its stochastic model. Transportation research part B: methodological 129, 334–350.
Treiber, M., Kesting, A., 2013. Traffic Flow Dynamics - Data, Models and Simulation. Springer.
Wang, M., Daamen, W., Hoogendoorn, S.P., van Arem, B., 2012. Driver assistance systems modeling by model predictive control. In: 2012 15th International IEEE Conference on Intelligent Transportation Systems. IEEE, pp. 1543–1548.
Wang, M., Daamen, W., Hoogendoorn, S.P., van Arem, B., 2015. Cooperative car-following control: Distributed algorithm and impact on moving jam features. IEEE Trans. Intell. Transp. Syst. 17 (5), 1459–1471.
Wang, M., Daamen, W., Hoogendoorn, S.P., van Arem, B., 2016. Connected variable speed limits control and car-following control with vehicle-infrastructure communication to resolve stop-and-go waves. Journal of Intelligent Transportation Systems 20 (6), 559–572.
Wang, Y., Zhang, Y., Hu, J., Li, L., 2012. Using variable speed limits to eliminate wide moving jams: a study based on three-phase traffic theory. Int. J. Mod. Phys. C 23 (09), 1250060.
Yuan, K., Knoop, V.L., Hoogendoorn, S.P., 2015. Capacity drop: Relationship between speed in congestion and the queue discharge rate. Transp. Res. Rec. 2491 (1), 72–80.
Yuan, Y., Van Lint, J., Wilson, R.E., van Wageningen-Kessels, F., Hoogendoorn, S.P., 2012. Real-time lagrangian traffic state estimator for freeways. IEEE Trans. Intell. Transp. Syst. 13 (1), 59–70.